2023-01-0235

Isolated Low Temperature Heat Release in Spark Ignition Engines

Samuel P. White, Abdullah U. Bajwa, Felix C.P. Leach
Department of Engineering Science, University of Oxford, UK

Abstract

Low temperature heat release (LTHR) has been of interest to researchers for its potential to mitigate knock in spark ignition (SI) engines and control auto-ignition in advanced compression ignition (ACI) engines. Previous studies have identified and investigated LTHR in both ACI and SI engines before the main high temperature heat release (HTHR) event by appropriately curating the in-cylinder thermal state during compression, or in the case of SI engines, timing the spark discharge late to reveal LTHR (sometimes referred to as pre-spark heat release). In this work, LTHR is demonstrated in isolation from HTHR events. Tests were run on motored single-cylinder engines and inlet air temperatures and pressures were adjusted to realise LTHR from n-heptane and iso-octane (2,2,4-trimethylpentane) without entering the HTHR regime. LTHR was observed for a lean n-heptane-air mixture at inlet temperatures ranging from 60°C to 100°C and inlet pressures of 0.9 bar (absolute). For temperatures below 60°C LTHR was not detected and for temperatures above 100°C measurements could not be taken due to the presence of HTHR. No LTHR was detected for iso-octane at 0.9 bar inlet pressures for the same conditions. Following predictions from chemical kinetics modelling in CHEMKIN (and previous studies), intake pressures were increased to 1.1 bar and 1.5 bar, which successfully led to the realisation of LTHR from iso-octane. The effect of temperature, pressure, and engine speed on the presence, intensity and phasing of LTHR are presented alongside pressure-temperature trajectories of the in-cylinder gases to explain the trends.

Introduction

Ever-increasing global CO_2 emissions mean that every effort must be made to reduce them as swiftly as possible. One technique, which can increase the efficiency of internal combustion engines (ICEs) by 10-20%, is lean operation - where the air:fuel ratio is weak of stoichiometric [1]. This improves the ratio of specific heats and leads to an efficiency improvement, provided the fuel-air mixture can still be ignited successfully. However, NO_x emissions need to be addressed either in-cylinder [2] or by exhaust aftertreatment (both of which can come with an efficiency penalty). One potential enabler for this technology, improving the ignition of the fuel-air mixture, is low temperature heat release (LTHR).

Certain fuels are known to possess two-stage autoignition (AI) chemistry, with non-monotonic relationships between mixture temperature and ignition delay due to negative temperature coefficient (NTC) behaviour [3]. The first heat release (HR) stage for such fuels, commonly referred to as low temperature heat release as it occurs at relatively low temperatures (< 850 K), has garnered interest recently because of its potential to promote clean and efficient combustion. Straight chain fuels like n-heptane and n-hexane exhibit stronger LTHR behaviour than branched chain species like iso-octane [4].

LTHR has been observed in internal combustion engines such as in controlled autoignition engines, where thermal conditions and fuel metering were managed to realise LTHR before the main volumetric autoignition stage [5, 6]. LTHR has also been observed in spark ignition (SI) engines as 'pre-spark heat release' (PSHR) induced by retarding spark timing, resulting in LTHR around top dead centre (TDC) before a spark discharge triggers deflagrative combustion [5, 7, 8].

A notable challenge in conducting experimental LTHR research is the coupled nature of low and high temperature heat release (HTHR) stages, whereby the former is obscured (to varying degrees) by the more dominant HTHR stage under 'firing' engine conditions. It has been suggested that LTHR could occur during deflagration [7], though distinguishing it from concurrent HTHR would require methods beyond pressure-based heat release analysis.

Strategies have been devised to bridge this gap: heuristic post-processing approaches have been used to isolate LTHR and HTHR portions from concurrent LTHR-HTHR data. Splitter et al. [7] used 'spline fitting' to estimate LTHR and HTHR contributions in an SI engine undergoing intermediate HR (when LTHR is partially revealed and lacks a distinct NTC drop). Waqas et al. [5] used heat release rate thresholds to define 'early heat release' in a controlled auto ignition (CAI) engine undergoing intermediate HR.

LTHR could potentially be controlled and harnessed to improve overall efficiency of internal combustion engines via the following methods:

- Improved understanding of end gas AI chemistry can help avoid abnormal combustion events like knocking and low-speed pre-ignition (stochastic pre-ignition) in spark ignition (SI) engines. This can enable engine operation at high boost levels, allow design of high compression ratio engines, and permit engine operation at thermodynamically efficient (advanced) spark timings. For fuels with significant NTC behaviour LTHR has been found to make knock onset less sensitive to inlet temperature by moving the mixture's thermodynamic state into a long-ignition-delay region [7]. Moreover, low-speed pre-ignition frequency and intensity have been found to be correlated to LTHR magnitude [9].
- Control of advanced compression ignition combustion by

utilising the thermal and chemical couplings between LTHR and HTHR processes in CAI engines, Shibata et al. [6] found LTHR and HTHR 50% mass fraction burned points (CA50) to be linearly related. Controlled autoigition has been shown to enable stable ultra-lean combustion [10] and so better control of autoignition using through improved understanding of the LTHR chemistry could expand the range of fuels and scenarios where ultra lean combustion can be utilised.

- Combustion efficiency improvements by tailoring end gas conditions to consume fuel via LTHR. It has also been hypothesised that LTHR-induced changes in mixture composition increase its laminar flame speed, which accelerates combustion [11]. This, if found to be true, can be another mechanism through which LTHR can improve combustion efficiency. Such improvements can promote ultra-lean combustion in spark ignition engines.

Isolated LTHR investigations can offer the following benefits:

- Chemical kinetics model validation and development to better represent the thermokinetics of LTHR reactions as emissions measured from isolated LTHR experiments will not be confounded by HTHR reactions. DelVescovo et al. [8] reported that existing chemical mechanisms have high levels of discrepancy even for a well-studied fuel such as iso-octane.
- Using appropriate ignition delay (ID), pressure and temperature surfaces, pressure-temperature (P-T) trajectories that lead to anomalous HTHR events can be studied and the underlying thermodynamic reasons for the breaches can be investigated.
- Relatively extreme LTHR conditions, which if accompanied by HTHR can be detrimental in SI engines, can be investigated. Improved understanding of chemical and thermodynamic conditions in the lead up to damaging HTHR events.
- For conditions where LTHR is weak, heat release based indexing of LTHR (for example, finding the crank angle at 2% mass fraction burned [7]) may not be sensitive enough to detect its onset. Studying LTHR in isolation allows weak LTHR to be detected using alternative methods, such as measurements of emissions or exhaust temperature.
- By separating LTHR from autoignition and deflagration, it can be investigated with minimal chemical and charge heating effects from residual gases.

This work demonstrates an experimental technique that decouples the two heat release regimes and allows the realisation of LTHR without a following HTHR stage. This is achieved by motoring a relatively low compression ratio gasoline direct injection (GDI) engine at elevated intake temperatures and, if need be, pressures to induce LTHR reactions.

Methodology

Quantifying LTHR

To measure and quantify the amount of energy release from low temperature heat release, net apparent heat release rate (AHRR), $\frac{\mathrm{d}Q_\mathrm{n}}{\mathrm{d}\theta}$ (defined as the heat release rate $\frac{\mathrm{d}Q_\mathrm{hr}}{\mathrm{d}\theta}$ less the heat transfer rate $\frac{\mathrm{d}Q_\mathrm{ht}}{\mathrm{d}\theta}$) was calculated in MATLAB using the crank angle (θ) based pressure p and volume V (calculated from engine geometry) traces according to Equation 1 [12], using a constant ratio of specific heats $\gamma = 1.35$:

$$\frac{\mathrm{d}Q_\mathrm{n}}{\mathrm{d}\theta} = \frac{\mathrm{d}Q_\mathrm{hr}}{\mathrm{d}\theta} - \frac{\mathrm{d}Q_\mathrm{ht}}{\mathrm{d}\theta} = \frac{\gamma}{\gamma - 1} p \frac{\mathrm{d}V}{\mathrm{d}\theta} + \frac{1}{\gamma - 1} V \frac{\mathrm{d}p}{\mathrm{d}\theta} \qquad (1)$$

To isolate heat release Q_hr measurements originating from LTHR from heat transfer Q_ht effects and other assumptions, the calculated AHRR trace for a corresponding unfuelled, motored case was subtracted from the fuelled case. Start of LTHR (SoLTHR) was determined by finding points around top dead centre (TDC) where either the AHRR of the fuelled and unfuelled cases deviated from each other or there was a noticeable inflection in the fuelled curve indicating HR onset. End of LTHR (EoLTHR) was identified as the point where the fuelled and unfuelled AHRR curves intersected again. The difference in AHRR was then integrated between these boundaries to find the total heat release in Joules per cycle, as shown in Figure 1.

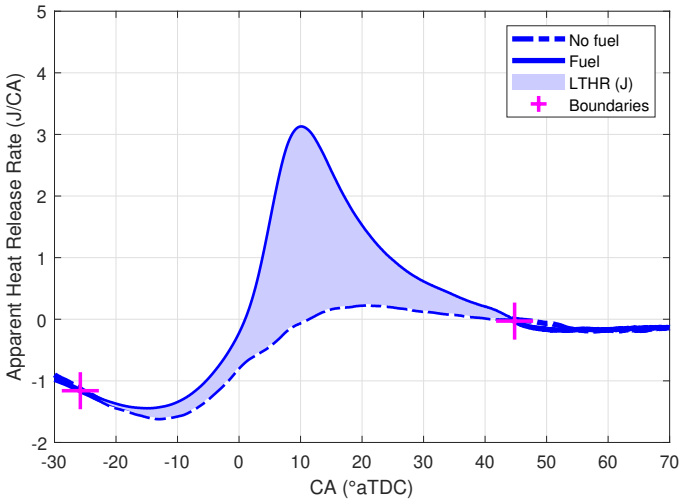

Figure 1: The difference between the apparent heat release rate fuelled and unfuelled test, with the quantity of LTHR highlighted in the shaded region

Cylinder temperature was calculated using the ideal gas law with measurements of cylinder pressure, cylinder volume and estimations of cylinder contents.

Experimental facility

The experimental work was conducted on two single cylinder internal combustion engines, one naturally aspirated, and another with the capability for boosted inlet air.

Single cylinder engine with optical access

For naturally aspirated inlet pressure conditions, a single cylinder, GDI research engine with the capability for optical access was used. The engine is referred to as the 'optical engine' due to the engine's capabilities, despite the fact that no optical diagnostic techniques were used in this work; its technical specifications are summarised in Table 1 and the engine has been fully described in previous work [13]. The engine was coupled with a Control Techniques motoring

dynamometer, to control engine speed. Fuel was injected at 160 bar, with injection timing and duration controlled by a Berkeley Nucleonics BNC725 unit. Ignition was disabled by disconnecting the ignition coil's power supply and control signal. The optical engine uses polyamide-imide piston rings to achieve an oil-free combustion chamber; engine coolant was controlled to its standard operating temperature of 45°C (to minimise the risk of melting the piston rings). The inlet air heater was controlled using a relay connected to a West 6100+ temperature controller; the inlet temperature fluctuated by up to ± 3°C at the higher temperature operating points. The test cell was controlled by a Taylor DynPro2 system, which was also used for continuous data logging at 1 Hz. Cylinder pressure data was measured using a Kistler Type 6041A high speed pressure transducer, at a resolution of 0.1 °CA (crank angle), recorded with an AVL X-ion high speed data acquisition system. The cylinder pressure signal was pegged every cycle to a barrel pressure transducer, which was exposed to the combustion chamber around TDC. High speed data was collected for 300 cycles, with three independent runs conducted per operating point. If the live pressure trace readings indicated HTHR via visibly high peak pressures, fuel injection was disabled immediately to avoid engine damage.

Single cylinder engine

For studying high inlet pressure conditions, a single cylinder, GDI engine based on a Ricardo Hydra bottom end was used. The engine is referred to as the 'thermal engine' and its technical specifications are summarised in Table 1. The engine was coupled to a 57 kW AC motoring dynamometer (Vascat MAC-Q with ABB power electronics) that maintained required speed (± 1 rpm). Fuel injection settings (timing, duration, rail pressure) were controlled by a Schaeffler Protronic ECU via an ETAS INCA interface. As with the optical engine study, ignition was disabled. The engine was operated at wide open throttle and intake pressure was increased to desired levels using a closed loop external boosting rig. Intake air was heated using a 10 kW electric heater (OSRAM Sylvania) installed upstream of the throttle valve and intake plenum.

The test cell has been fully described in previous publications [14, 15, 16]. Inlet pressure was measured around 35 cm upstream of the inlet ports using a Druck UNIK 5000 series sensor and logged at a frequency of 1 Hz using a Sierra-CP CADET engine control system. Temperatures (measured using 3mm k-type thermocouples), fuel flow rate (measured using a coriolis flow meter, Siemens FC Mass 2100), air flow rate (measured using a hot wire flow meter, Sierra-CP Airtrak 628S), and exhaust composition (measured using a Horiba MEXA-ONE) were also recorded at 1 Hz. Cylinder pressure was measured using a water-cooled piezoelectric transducer (Kistler-6041B) and was logged, along with other high-speed measurements (manifold pressures, valve lift), at a resolution of 0.1 °CA using a high-speed data acquisition system (AVL Indiset). Data post-processing was performed using AVL Concerto and custom MATLAB scripts.

Engine coolant and oil temperatures were maintained at 90°C during experiments using closed loop temperature control systems within 2 and 1°C, respectively. Slow and high-speed data were recorded for 30 seconds and 300 cycles, respectively.

Parameters	Optical	Thermal
Bore [mm]	89.0	83.0
Stroke [mm]	90.3	92.0
Displacement [cm^3]	561.9	500.0
Compression ratio	11.1:1	10.56:1
Valves per cylinder	2 intake, 2 exhaust	
Fuel injection system	Direct injection	Direct injection production injector centrally mounted in cylinder head

Table 1: Engine specifications.

Operating conditions

n-Heptane tests

Engine parameters used are listed in Table 2. Inlet temperature sweeps were carried out with inlet pressure and injection duration held constant. As a result air mass flow rate and hence equivalence ratio varied with inlet temperature. Equivalence ratio (ϕ) was estimated by using fuel flow rate measurements from a calibration of the injector, using a lambda sensor close to its stoichiometric operating point.

Iso-octane tests

Tests were performed with iso-octane at a constant equivalence ratio of 0.5 at three speeds, four inlet temperatures and two inlet pressures (Table 2). Equivalence ratios, calculated from fuel and air flow measurements and verified from exhaust emissions using the 'Spindt' method [17], were maintained between 0.48 and 0.5. Inlet temperatures were maintained within ± 2°C and pressure within ± 0.01 bar.

Parameters	Optical	Thermal
IVO [°CA aTDC]	-336	-352
IVC [°CA aTDC]	-86	-165
EVO [°CA aTDC]	116	159
EVC [°CA aTDC]	366	359
Speed [rpm]	1100	1000, 1500, 2000
Injection pressure [bar]	160	140
Injection timing [°CA aTDC]	-270	-300
Inlet temperature [°C]	40, 60, 80, 100	60, 80, 100, 120
Inlet pressure [bar (absolute)]	0.9	1.1, 1.5
Equivalence ratio (ϕ)	0.5	0.5
Fuel	n-heptane (>99% purity)	iso-octane (>99% purity)

Table 2: Engine settings.

Modelling

Ignition delay simulations were performed in CHEMKIN, using the closed homogeneous ignition delay model with a constant volume. The simulations modelled 200 ms of reactions, and reported ignition delay defined by a 50 K rise in temperature, in order to detect the relatively small changes in temperature due to LTHR. Mixtures of air and both n-heptane and iso-octane were modelled at an equivalence ratio of 0.5 using a reduced Lawrence Livermore National Laboratory gasoline surrogate mechanism [18].

Results and Discussion

Isolated LTHR

Isolated LTHR from n-heptane the optical engine is shown Fig. 2. The figure shows calculated apparent heat release rate for the optical engine with heated intake at 100°C for cases with and without n-heptane injected. Heat release for the case with n-heptane deviates from the motored air case, exceeding 4 J/°CA around 8 °after TDC (aTDC). Fig. 3 shows the pressure rise due to the heat release, from which AHRR was calculated. Peak cylinder pressure was only marginally higher than the non-fuelled case, but occurred at a later crank angle. There was no evidence of HTHR, i.e. there were no rapid pressure rises and the overall magnitude of heat release remained low.

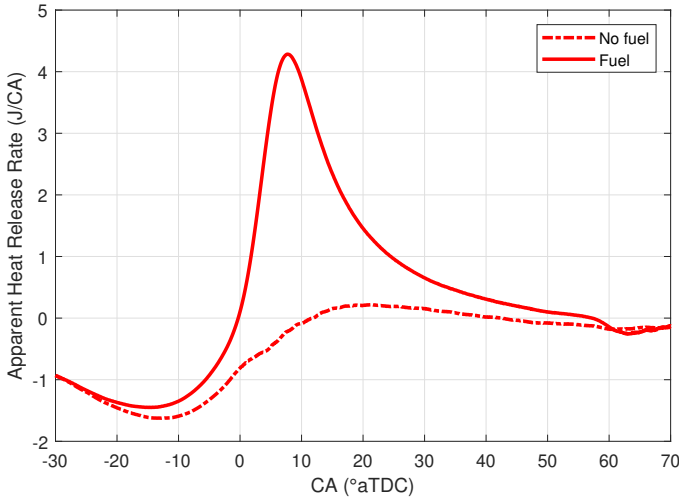

Figure 2: AHRR traces for an engine motored with and without n-heptane, with inlet air heated to 100°C

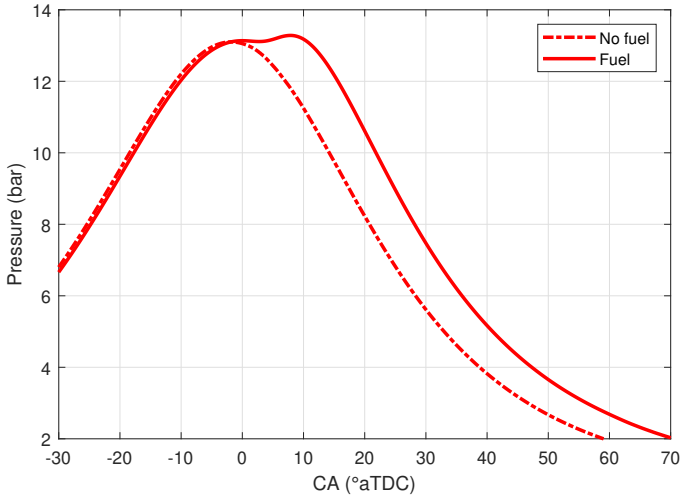

Figure 3: Pressure traces for an engine motored with and without n-heptane, with inlet air heated to 100°C

Temperature effects on LTHR in n-heptane

LTHR was virtually non-existent when near-ambient (40°C) inlet temperatures (T_{in}) were used at the same conditions as in Fig. 2 and Fig. 3; This can be seen in Fig. 4 where the heat release trace of the fuelled case closely follows the non-fuelled case, and in Fig. 5 where the cylinder pressure was lower in the fuelled case. The slight difference in pressure may be accounted for by charge cooling effects of the direct injected fuel.

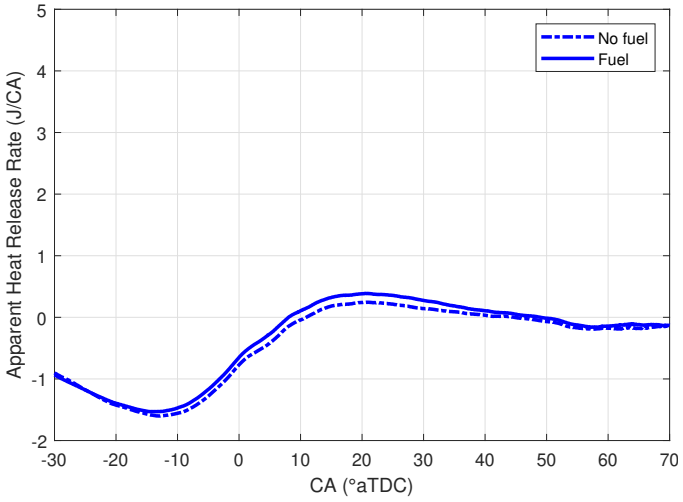

Figure 4: AHRR traces for an engine motored with and without n-heptane, with inlet air heated to 40°C

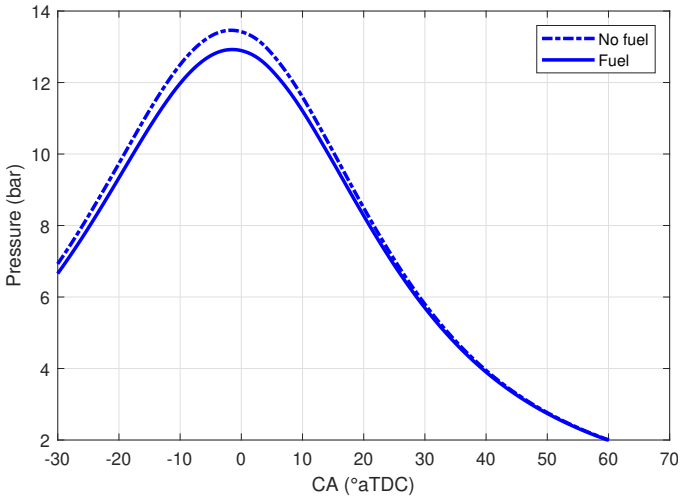

Figure 5: Pressure traces for an engine motored with and without n-heptane, with inlet air heated to 40°C

The effect of inlet temperature on the pressure traces of mixtures exhibiting LTHR can be examined in Fig. 6. The $T_{\text{in}} = 40°\text{C}$ case, and to a lesser extent the $T_{\text{in}} = 60°\text{C}$ case resemble a typical unfuelled, motoring pressure; however, as inlet temperature increases, the traces deviate from motoring after TDC, as a result of the pressure rise due to the heat released by low temperature reactions. The effect of LTHR on pressure traces is most noticeable for the $T_{\text{in}} = 100°\text{C}$ case, where pressure rises and peaks after TDC.

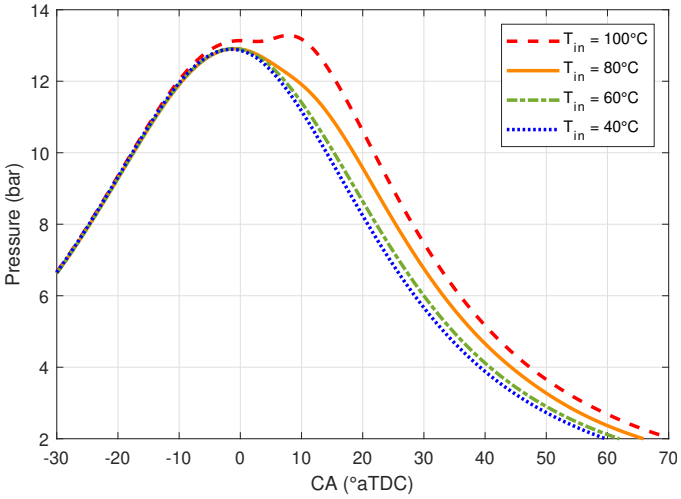

Figure 6: Pressure traces for an engine motored with n-heptane at range of inlet temperatures

Cylinder temperature traces are shown for the increasing inlet temperatures in Fig. 7. For the cases $T_{\text{in}} = 100°\text{C}$ and $T_{\text{in}} = 80°\text{C}$, a second peak in cylinder temperature occurs after TDC, caused by LTHR.

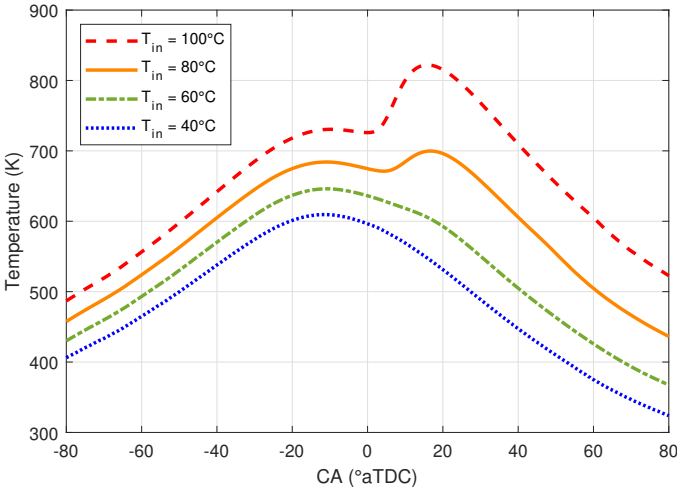

Figure 7: Temperature traces for an engine motored with n-heptane at range of inlet temperatures

Fig. 8 shows the clear effect of increasing inlet temperature on LTHR. The graph shows the difference in heat release rate compared to an unfuelled, motored case at the different inlet conditions. The magnitude of heat release increases from negligible at $T_{\text{in}} = 40°\text{C}$ to 4.5 J/°CA at the highest inlet temperature. The integral of apparent heat release rate, cumulative heat release (CHR) is shown in Fig. 9, which gives an indication of the increased magnitude of heat release from LTHR and advanced LTHR phasing as inlet temperature increases.

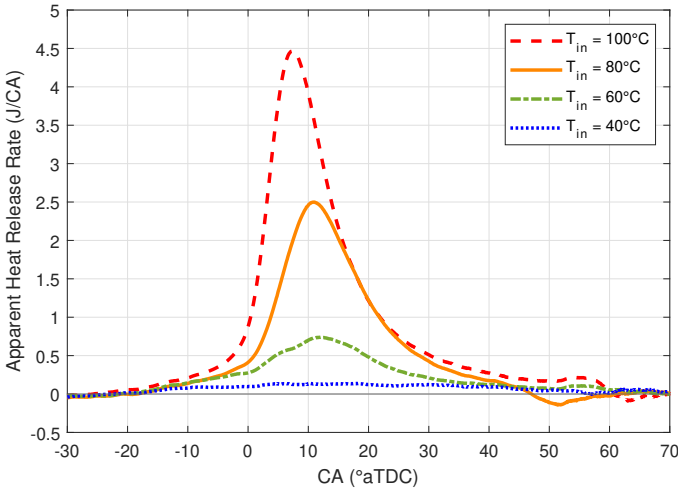

Figure 8: Apparent heat release rate traces for an engine motored with n-heptane at range of inlet temperatures

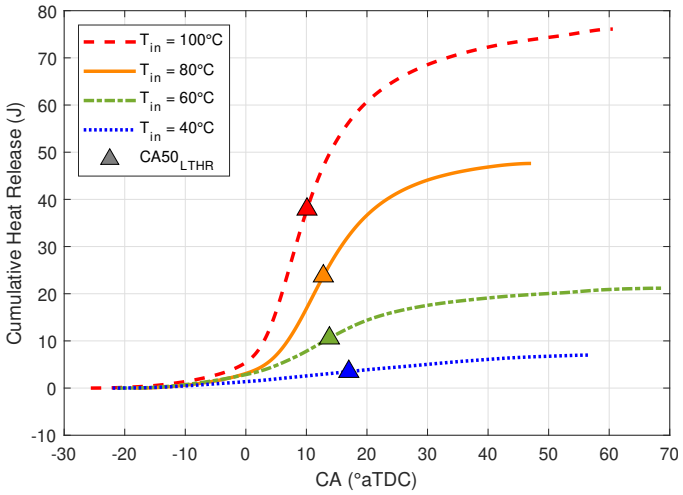

Figure 9: Cumulative heat release traces for an engine motored with n-heptane at range of inlet temperatures

The effect of inlet temperature on on total heat release from LTHR is shown in Fig. 10. There is a clear trend in increasing quantity of heat release with increasing inlet temperature, from near zero at $T_{\text{in}} = 40°\text{C}$ to around 65 J per cycle for $T_{\text{in}} = 100°\text{C}$. This can be explained by the analysing pressure-temperature (P-T) trajectories through the ignition delay contour in Fig. 11, which shows a contour of n-heptane ignition delay as defined by a 50K rise in temperature [7]. For the $T_{\text{in}} = 40°\text{C}$ case, the P-T trajectory only traverses portions of the ignition delay contour with ignition delay less than 0.1 s for a brief period, and in that brief period the value of the ignition delay is relatively long. As inlet temperature increases, the respective P-T trajectories shift right into higher temperature regions where ignition delay is reduced. The longer the time the mixture's thermodynamic state resides in the shorter ignition region, the more opportunity there is for chemical reactions that result in LTHR. The compression trajectory of the $T_{\text{in}} = 100°\text{C}$ case takes it into regions of very short ignition delay, explaining the earlier and greater LTHR. The effect of LTHR on the trajectory can be seen in the plots: there is a clear rise in temperature at near constant pressure for the $T_{\text{in}} = 100°\text{C}$ case and a more delayed and gradual rise in temperature for the $T_{\text{in}} = 80°\text{C}$ case as pressure decreases during its expansion stroke.

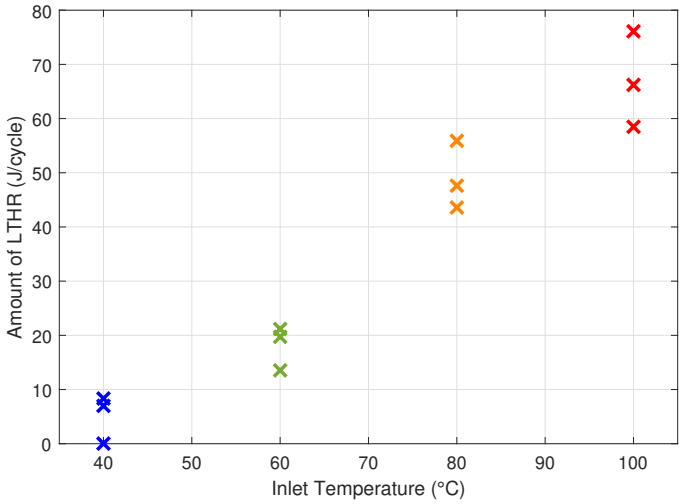

Figure 10: Amount of LTHR per cycle from n-heptane against inlet temperature

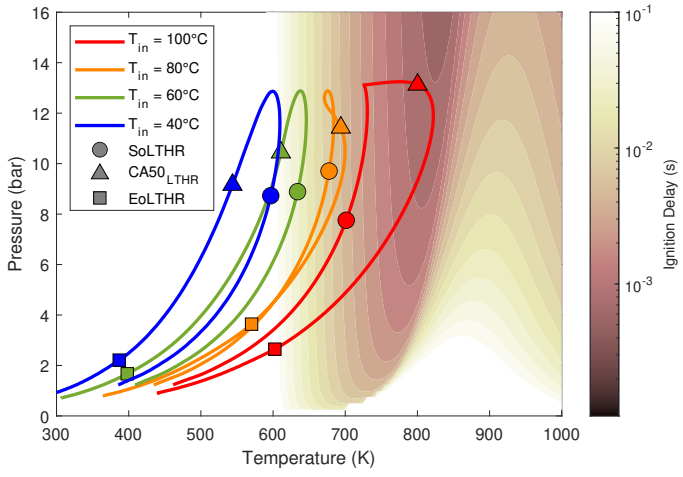

Figure 11: Pressure-temperature trajctories of cycles from an engine motored with n-heptane at range of inlet temperatures superposed onto an ignition delay contour for n-heptane, defined by 50 K rise in temperature

The time (t) spent traversing through the contour of varying ignition delay (τ) can be summarised by the Livengood-Wu (LW) integral, to give an estimate of overall progression towards the ignition delay time (Equation 2).

$$\text{LW} = \int_0^t \frac{dt}{\tau\left(T\left(t\right), P\left(t\right)\right)} \tag{2}$$

This is represented by the solid lines in Fig. 12. A LW score of above unity suggests that, on average, the mixture reached its ignition point (as defined by a 50 K rise in temperature) and measurable heat release as a result would be likely. The two cases where the LW score did not reach 1 ($T_{\text{in}} = 60°\text{C}$ and $T_{\text{in}} = 40°\text{C}$) also exhibited some heat release; this may be explained by two factors: temperature stratification and the possibility of autoignition reactions that lead to a temperature rise of less than 50 K that are not accounted for by the ignition delay contour upon which the calculation is based. The dashed lines represent the reciprocal of instantaneous ignition delay of the mixture, ($\frac{1}{\tau}$) and give an indication of when during the cycle the mixture was traversing through regions of short ignition delay.

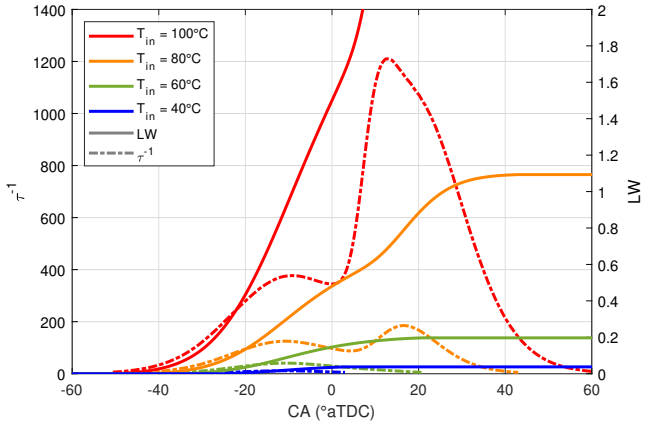

Figure 12: Livengood-Wu (LW) integral score traces for an engine motored with n-heptane at range of inlet temperatures

The effect of inlet temperature on LTHR phasing can be shown in Fig. 13. One of the data points for $T_{\text{in}} = 40°\text{C}$ is omitted as no LTHR was detected. Increased inlet temperature resulted in more advanced phasing of the 50% LTHR point (the point at which half of the energy from LTHR has been released). This can be explained by analysing P-T trajectories through the ignition delay contour in Fig. 11 and by $\frac{1}{\tau}$ in Fig. 12; the thermodynamic state of the mixtures that began with higher inlet temperatures reach the short ignition delay region sooner and therefore LTHR begins sooner, when compared to the lower inlet temperature cases.

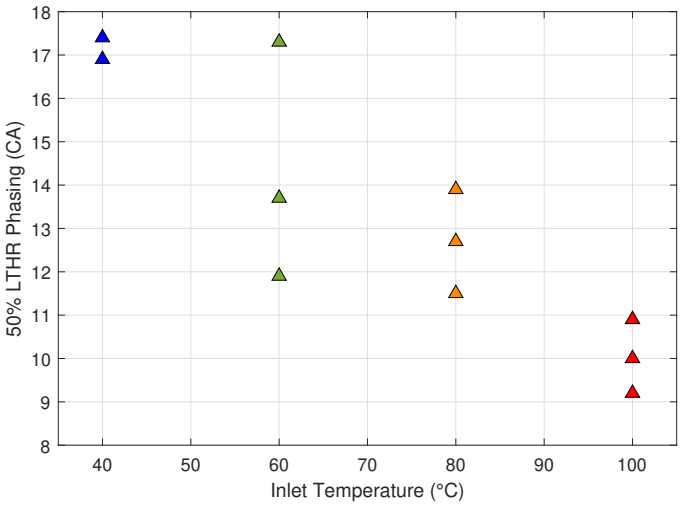

Figure 13: Phasing of 50% LTHR from n-Hepate against inlet temperature

LTHR vs HTHR

Data collection was hindered for inlet temperatures above 100°C due to the onset of high temperature heat release. Fuel injection had to be cut to avoid damage to the apparatus. However, some cycles were captured for a case ($T_{\text{in}} = 140$°C) at the same inlet pressure and with shorter injection duration compared to the rest of the data (0.85 ms versus 1 ms) that contain a period of around 60 consecutive HTHR cycles amongst 300 LTHR cycles. Figs. 14, 15 and 16 show the cycles plotted separately alongside a corresponding unfuelled case, and highlights the difference between the two phenomena. The two distinct periods of heat release, peaking at -12 °CA and 10 °CA can be seen in the HTHR + LTHR trace in Fig. 14; these separate heat release events originated from a single fuel injection and no external ignition source. HTHR + LTHR trace closely resembles traditional HCCI heat release behaviour from Urushihara et. al [19]. The phasing of the LTHR was earlier in the cycles where HTHR was present (-12 °CA vs 3 °CA); reasons for this could include higher cylinder temperatures from previous HTHR cycles, or residual combustion products changing the chemical pathways and accelerating the LTHR onset. The temperature traces in Fig. 16 clearly show the two-stage autoignition behaviour commonly exhibited by alkane fuels such as n-heptane; two rapid rises in temperature can be seen at -12 °CA and 10 °CA, with the NTC region occurring at 925 K. Fig. 15 shows the pressure traces for the two cases, with peak pressure for LTHR only occurring approximately 2 °CA after the unfuelled case at 14.5 bar, whilst the HTHR case peaked much later at 14 °CA with a peak pressure of 21.5 bar. The onset and retreat of HTHR cycles were both sudden. The sudden onset was likely caused by minor variations in residuals and slightly unsteady inlet air temperature which led to the initial cylinder temperature crossing an HTHR threshold during a given cycle. This may have become unsustainable when HTHR stopped due to the unsteady inlet air temperatures decreasing again.

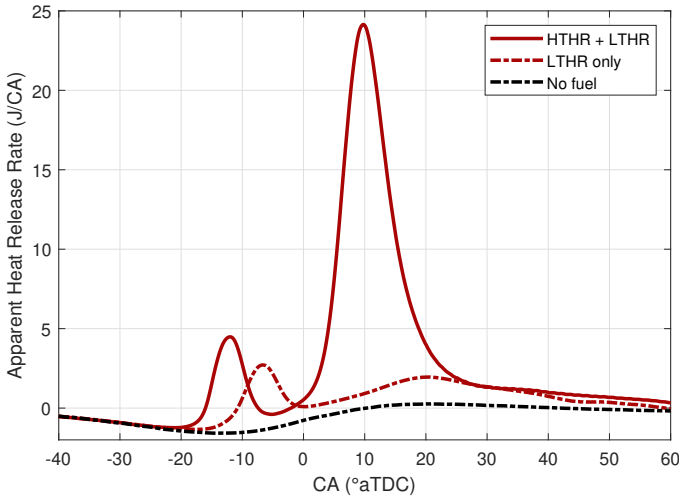

Figure 14: AHRR traces of HTHR vs isolated LTHR

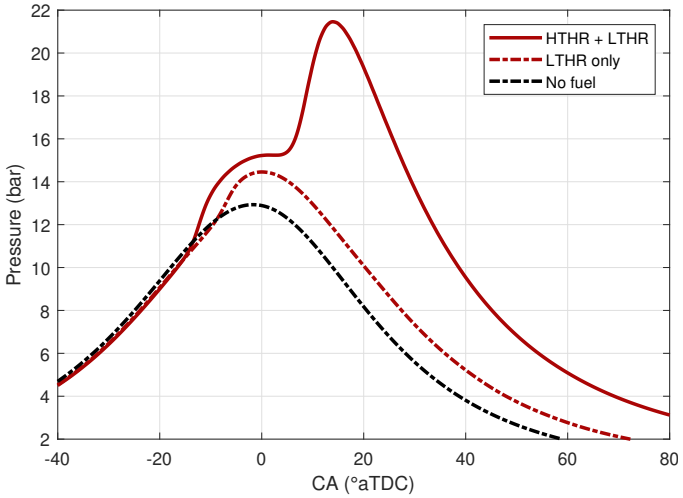

Figure 15: Pressure traces of HTHR vs isolated LTHR

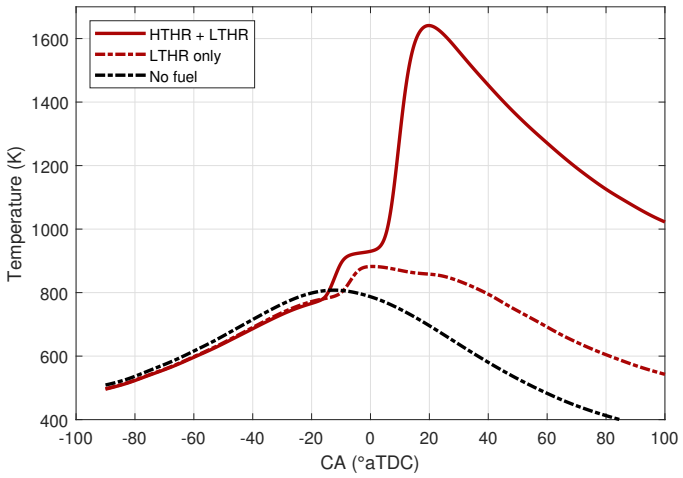

Figure 16: Temperature traces of HTHR vs isolated LTHR

Isolated LTHR with iso-octane

Isolated LTHR was successfully observed with iso-octane on the thermal engine at 1000 rpm with boosted inlet conditions (1.5 bar) at an inlet temperature of 60°C. Sample LTHR results are shown in Fig. 17 and Fig. 18 as cylinder pressure and heat release curves, respectively.

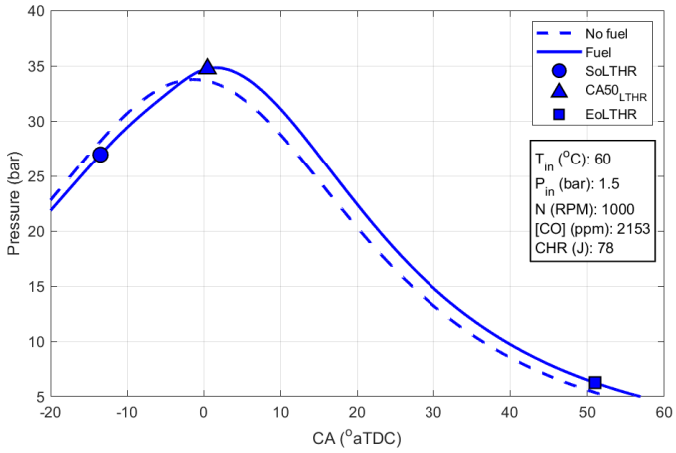

Figure 17: Pressure traces for the thermal engine motored with and without iso-octane at $T_{\text{in}} = 60°\text{C}$

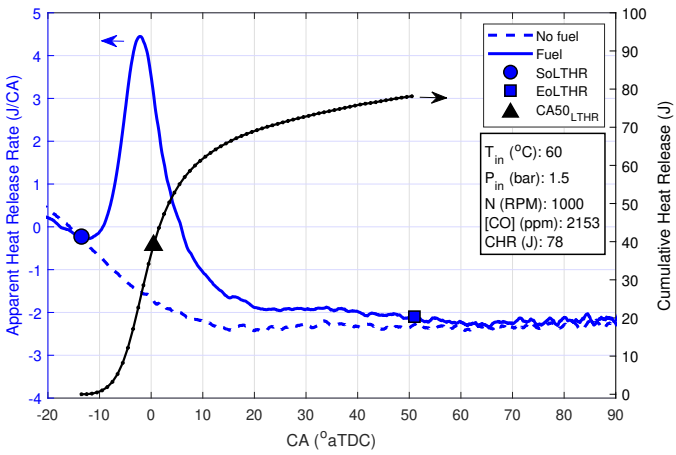

Figure 18: AHRR traces for the thermal engine motored with and without iso-octane at $T_{\text{in}} = 60°\text{C}$

Estimated cylinder temperature and measured pressure for the above data point are shown in Fig. 19 with various LTHR milestones marked. The cylinder mixture's thermal state rests in the LT region (first region of short ID, T $<$ 800 K) at the start of HR. The P-T trajectory shows that ID initially decreases but progressive HR causes it to increase despite the accompanying rise in cylinder temperature (i.e. NTC behaviour), which eventually causes HR to cease. In following sections, the effect of changing engine inlet conditions and speed on iso-octane LTHR is discussed by analysing shifts in P-T trajectories.

LTHR vs HTHR

LTHR experiments at 1000 rpm and boosted conditions were prone to extreme and inconsistent HTHR events, especially as inlet temperatures increased beyond 70°C. Sample HTHR results are shown in Fig. 20, which contains 25 consecutive HTHR cycles and 25 HTHR-preceding LTHR cycles. Once HTHR started, combustion did not return to the LTHR regime and fuel injection had to be stopped to prevent damage to the engine. Therefore, only a limited amount of

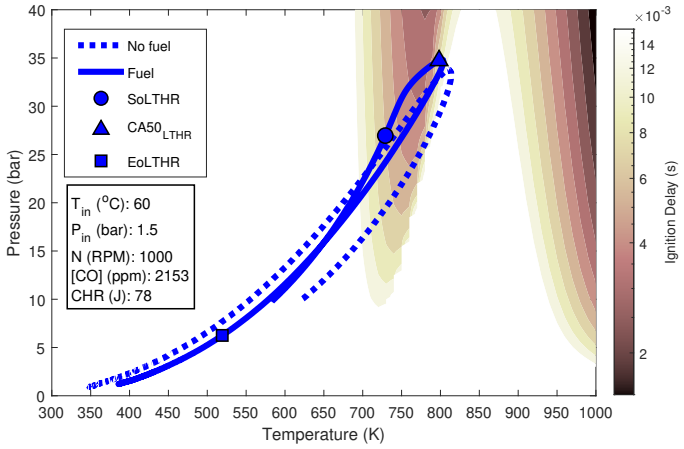

Figure 19: P-T trajectories of cycles from the thermal engine motored with and without iso-octane at $T_{\text{in}} = 60°\text{C}$

iso-octane LTHR data is available at 1000 rpm, which is used in the next section to to discuss the effects of time availability on LTHR.

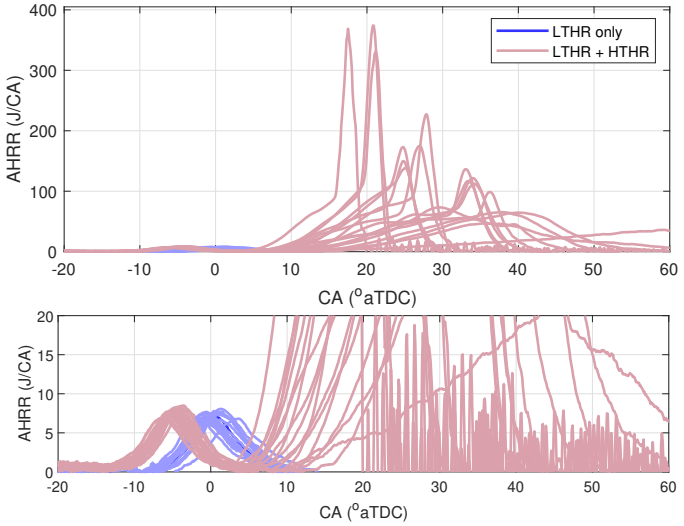

Figure 20: Sample iso-octane HTHR results at $T_{\text{in}} = 80°\text{C}$, $P_{\text{in}} = 1.5$ bar, and $\phi = 0.75$. Bottom subplot is a magnified version to highlight LTHR cycles

The occurrence of HTHR can be attributed to the simultaneous (volumetric) HR across the cylinder for a relatively long period of time that increased cylinder temperature sufficiently to shift the mixture state rightward in the P-T space from the LT to the HT region. It can be speculated that after the onset of HTHR, compression P-T trajectories shifted to further higher temperatures because of the presence of hot residual gases. This might explain the apparent irreversible nature of the shift from LTHR to HTHR. Chemical reformation during the relatively long LTHR period could have also changed mixture ID characteristics and contributed to HTHR occurrence. The observed extreme HTHR cycles can be categorised as low-speed pre-ignition, which is known to exhibit LTHR [9] and will be investigated further in future studies using engine chemical kinetics simulation models. LTHR experiments at 1000 rpm in Splitter et al. [7] were also limited to 90°C T_{in} by pre-ignition events.

Temperature effects on LTHR in iso-octane

Inlet temperatures were swept from 60 to 120°C at an inlet pressure of 1.5 bar and engine speed of 1500 rpm. Increasing inlet temperatures increased compression temperatures and decreased compression

pressures as shown in Fig. 21 and Fig. 22, respectively. Consequently, the mixture's P-T trajectories moved rightward (Fig. 23) and entered the LTHR short ID region earlier as marked by the red line in Fig. 21. The compression P-T trajectories for the high temperature cases, however, had longer effective ID (i.e. low LW score), which pushed their SoLTHR points close to the NTC region, causing them to land in the NTC region relatively quickly. Resultantly, the amount of energy released via LTHR at high inlet temperatures was limited as shown in the CHR results in Fig. 24. The measured increase in exhaust temperature, shown collectively for two inlet pressures in Fig. 25, demonstrates the same trends. The LTHR intensity trends are consistent with chemical kinetics modelling results from Pan et al. [20] that studied LTHR for n-heptane at different initial temperatures.

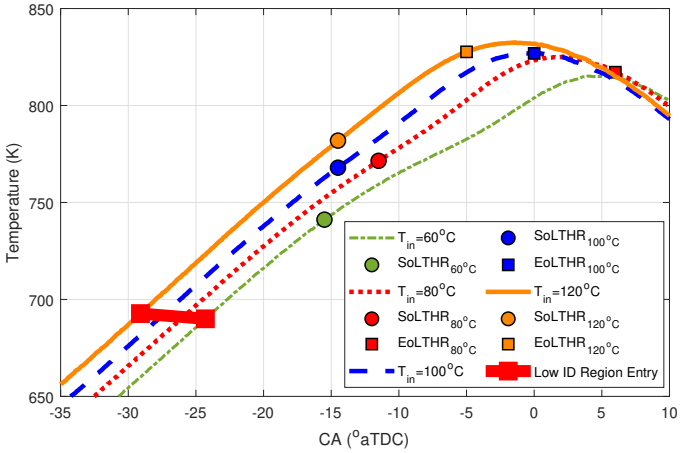

Figure 21: Cylinder temperature during compression and initial portion of LTHR at four inlet temperatures (P_{in} = 1.5 bar, 1500 rpm, ϕ = 0.5)

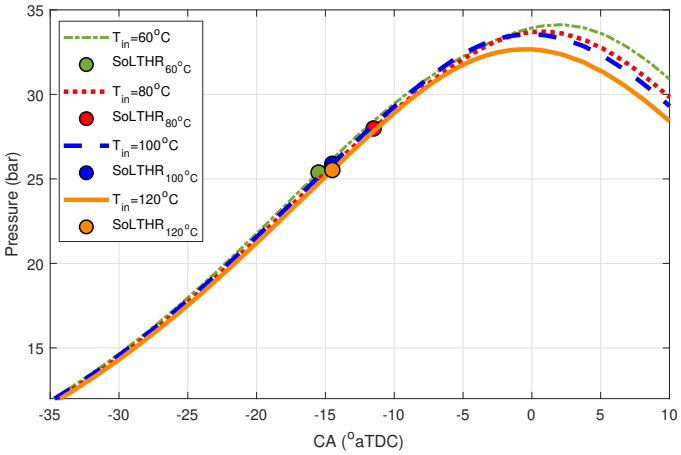

Figure 22: Cylinder pressure during compression and initial portion of LTHR at four inlet temperatures (P_{in} = 1.5 bar, 1500 rpm, ϕ = 0.5)

Figure 24 also shows that increasing inlet temperatures advances LTHR phasing (CA location at 50% heat release point - CA50). This observation is consistent with iso-octane PSHR experiments by Szybist and Splitter [21] in which relatively advanced LTHR, characterised by a distinct NTC drop and absence of merged LT-HT HR (intermediate HR), was observed at inlet temperatures above 90°C. The trends regarding the magnitude of LTHR (LTHR weakening at higher temperatures) are, however, opposite. This could be because in the PSHR experiments, a portion of LTHR was obscured by deflagrative HR. In a following study by Splitter et al. [7], inlet temperatures were increased to 180°C, and LTHR intensity was found to reduce beyond 120°C while the advancement of LTHR phasing continued. Waqas et al. [5] reported decreasing LTHR with increasing inlet temperature from 52 to 80°C in a cooperative fuel research engine at relatively low LTHR pressures (< 15 bar) for a PRF-90 fuel (a mixture of 10% (v/v) n-heptane and 90% iso-octane).

At elevated temperatures (T_{in} > 60°C), SoLTHR temperatures are nearly constant (Fig. 23). Temperatures at end of heat release are in close proximity as well. These observations might provide support to the idea that fuels with two-stage chemistry 'self-regulate' temperature rise during LTHR, which reduces SI engine knocking sensitivity to inlet temperature [7]. More data including at higher CHR levels will be needed to investigate this thoroughly.

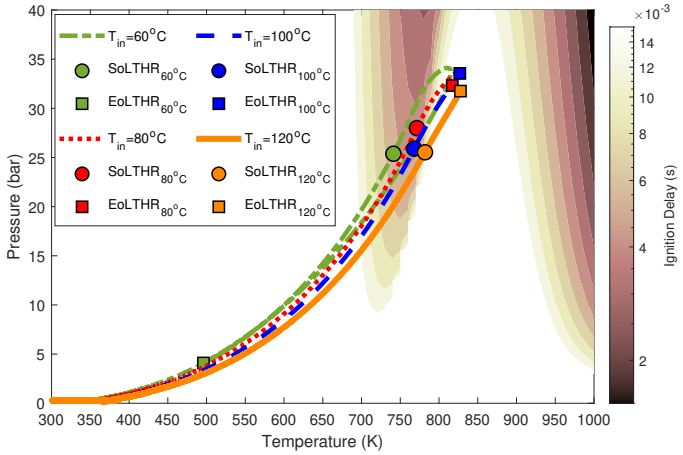

Figure 23: P-T trajectories during LTHR at four inlet temperatures (P_{in} = 1.5 bar, 1500 rpm, ϕ = 0.5)

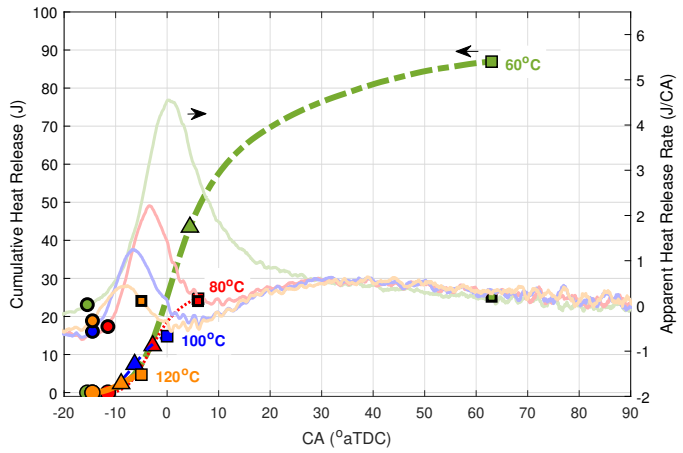

Figure 24: Cumulative (left) and rate of apparent heat release (right) at four inlet temperatures (P_{in} = 1.5 bar, 1500 rpm, ϕ = 0.5)

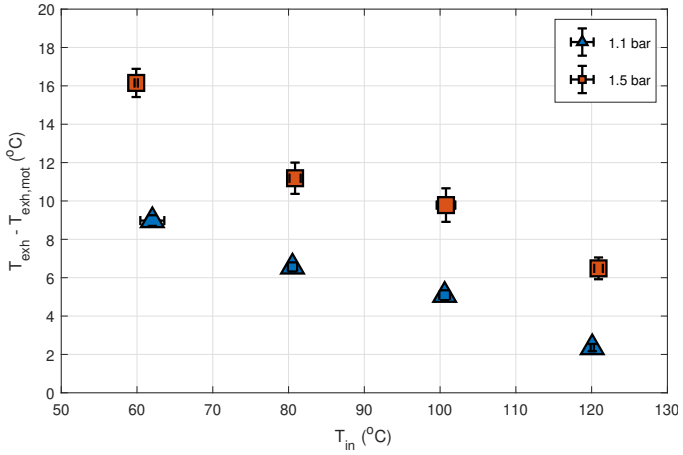

Figure 25: Change in LTHR strength (indexed by increase in exhaust temperature) with inlet temperature changes (P_{in} = 1.1 and 1.5 bar, 1500 rpm, ϕ = 0.5)

Pressure effects on LTHR in iso-octane

Inlet temperature sweep was repeated at an inlet pressure of 1.1 bar to assess the low pressure limits of iso-octane LTHR. LTHR was still observed but with significantly diminished intensity as shown in Fig. 25 and Fig. 26 by exhaust temperature and CHR results, respectively. The LTHR weakening can be attributed to elongation of the effective ID time (low LW scores) resulting from lowering of the P-T trajectories to low ID regions in Fig. 27. The trends with inlet temperature variations are the same as for 1.5 bar and can be explained using the same line of reasoning. At 120°C, no HR was detected from HR analysis but exhaust temperature results (Fig. 25) indicate weak signatures of LTHR, pointing at the limitations of AHRR based LTHR indexing. Exhaust based measurements and 'effective' ID time metrics like the LW score can potentially help provide higher resolution LTHR strength indexing.

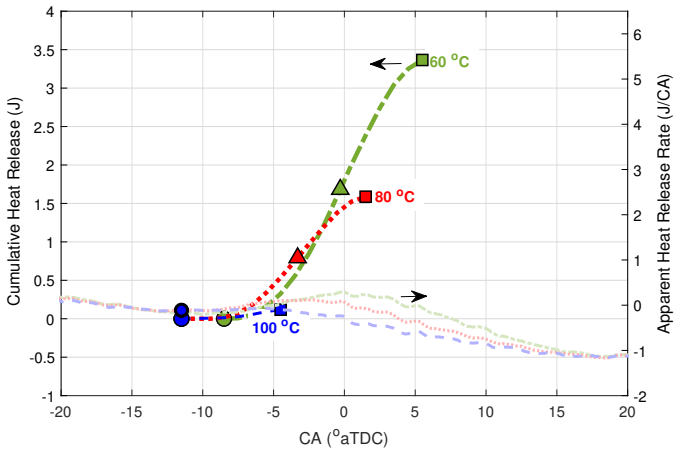

Figure 26: Cumulative LTHR at four inlet temperatures at $P_{in} = 1.1$ bar, 1500 rpm, and $\phi = 0.5$

Note: The motoring AHRR difference based method produced unrealistic results at such weak LTHR conditions, therefore, only the firing cycles were used in CHR computation.

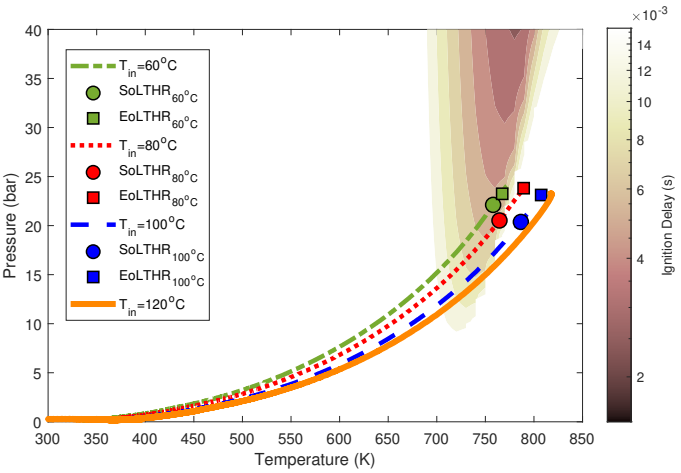

Figure 27: P-T trajectories during LTHR or compression in cases with no LTHR at four inlet temperatures ($P_{in} = 1.1$ bar, 1500 rpm, $\phi = 0.5$)

Engine speed effects on LTHR in iso-octane

Tests were performed at 1.5 bar inlet pressure and inlet temperatures of 60 and 80°C at 1000, 1500 and 2000 rpm.

Fig. 28 and Fig. 29 show the cylinder temperature and pressure for the three speed points, respectively. Increasing engine speed increased cylinder temperature because of reduced wall heat losses. The effect on pressure was less pronounced because of accompanying reductions in volumetric efficiency. The resulting effect on the mixture thermal state in the P-T space (Fig. 30) was a rightward shift whereby the compression P-T trajectories entered the LTHR short ID region earlier in the cycle (marked by the red line in Fig. 28). However, the time spent in the LTHR ID region was shorter for the higher speed cases which caused SoLTHR to occur at higher temperatures despite the mixture state traversing the low ID contours that initiated LTHR at 1000 rpm. In other words, though the cylinder mixture's thermal state existed in relatively low ID regions, it did not rest there long enough for sufficient LT reactions to 'build up' to yield sensible LTHR, i.e. the LW score was low.

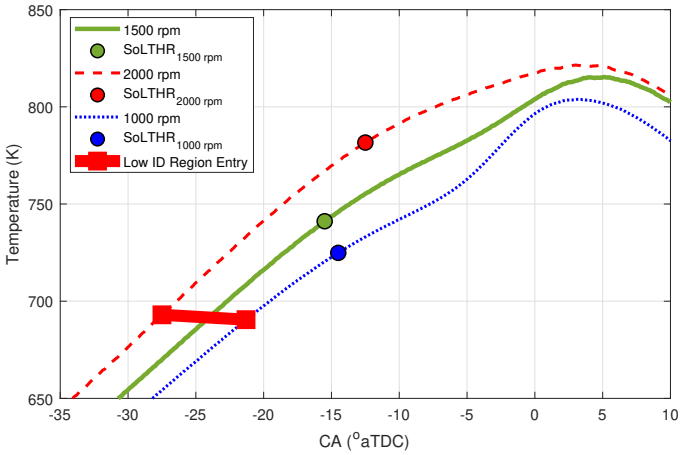

Figure 28: Cylinder temperature during compression and initial portion of LTHR at three engine speeds ($P_{in} = 1.5$ bar, $T_{in} = 60$°C, $\phi = 0.5$)

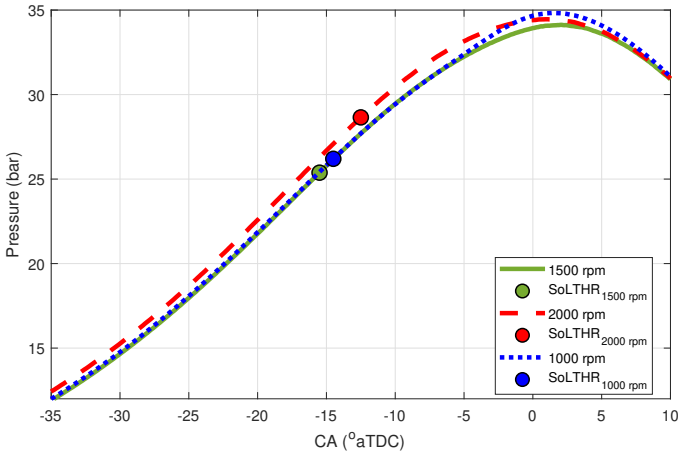

Figure 29: Cylinder pressure during compression and initial portion of LTHR at three engine speeds ($P_{in} = 1.5$ bar, $T_{in} = 60$°C, $\phi = 0.5$)

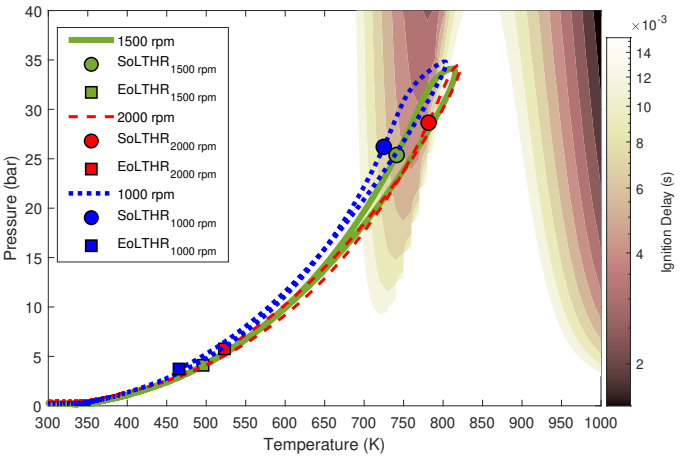

Figure 30: P-T trajectories during LTHR at three engine speeds ($P_{in} = 1.5$ bar, $T_{in} = 60°C$, $\phi = 0.5$)

The location of the SoLTHR points in Fig. 30 for the high speed cases was closer to the NTC region edge, and their respective post-SoLTHR P-T trajectories traversed relatively long ID regions. Resultantly, the total heat release amount was reduced, as can be seen from the AHRR results in Fig. 31. The LTHR intensity observations are also supported by measured rise in exhaust temperatures relative to motoring temperatures (Fig. 32). Such independent experimental indexing of LTHR strength is not possible in combined LTHR-HTHR experiments. Fig. 32 also contains results for 80°C inlet temperature experiments, which indicate a weakening effect of inlet temperatures increase on LTHR as discussed above. The retardation of LTHR phasing (CA50 in Fig. 31) with speed increase can also be explained by the differences in the effective ID times for the three speeds.

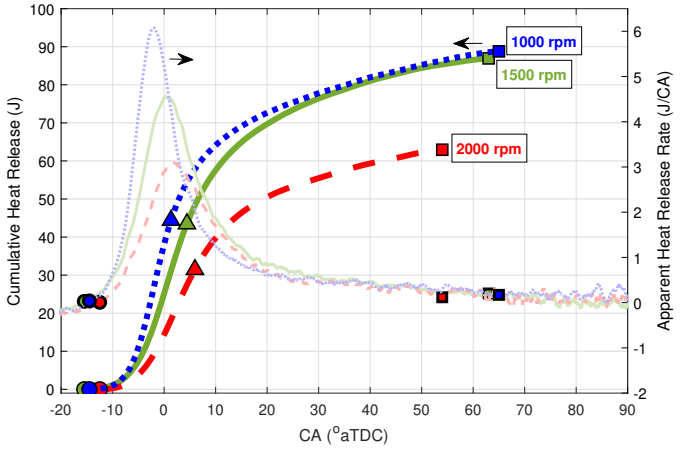

Figure 31: Cumulative (left) and rate of apparent heat release (right) at three engine speeds ($P_{in} = 1.5$ bar, $T_{in} = 60°C$, $\phi = 0.5$)

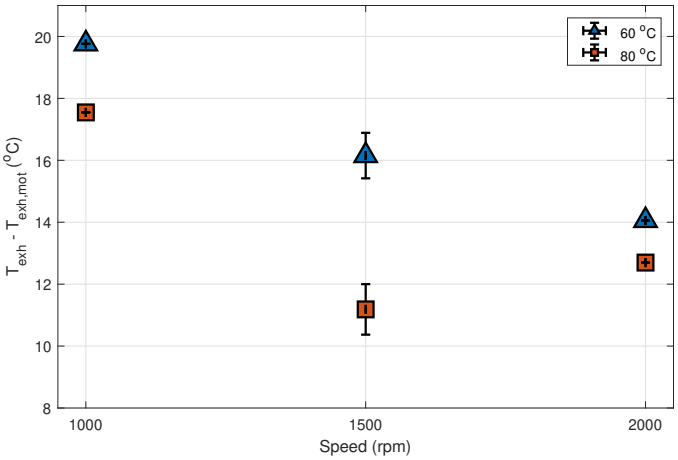

Figure 32: Change in LTHR strength (indexed by increase in exhaust temperature) with engine speed changes ($P_{in} = 1.5$ bar, $T_{in} = 60°C$ and $80°C$, $\phi = 0.5$)

Conclusions

This work has presented, for the first time, LTHR decoupled from HTHR using iso-octane and n-heptane as fuels in two different gasoline direct injection engines. The results showed the following:

1. It is possible to observe LTHR for n-heptane, a low octane number fuel in gasoline direct injection engines, without subsequent HTHR, when inlet heating is utilised.
2. With inlet heating and boosting, isolated LTHR can also be observed for iso-octane, a high octane number fuel.
3. The magnitude of heat release originating from LTHR can be measured by comparing the pressure derived AHRR measurements from a fuelled LTHR case to an unfuelled, motored case.
4. The effect of inlet temperature on isolated LTHR depends on the specific fuel's ignition delay characteristics, and the pressure and temperature conditions that the mixture traverses throughout its cycle. The more time the mixture resided in the short ignition delay (by 50 K rise) region, the more energy was released by LTHR.
5. The net effect of increasing inlet temperature for n-heptane and iso-octane were strengthening and weakening of LTHR, respectively. The changes in LTHR intensity for iso-octane are opposite to what has been reported in PSHR studies.
6. Increasing engine speed and decreasing inlet pressure reduced the amount of energy released through LT reactions because the changes in mixture's state reduced the effective low-ID region residence time.
7. Isolating LTHR allowed indexing of LTHR strength using out-of-cylinder measurements such as exhaust temperature.

Abbreviations

$\frac{dQ_{hr}}{d\theta}$	Heat release rate
$\frac{dQ_{ht}}{d\theta}$	Heat transfer rate
$\frac{dQ_{n}}{d\theta}$	Net apparent heat release rate
γ	Ratio of specific heats

ϕ	Equivalence ratio
τ	Ignition delay
θ	Crank angle
ACI	Advanced Compression Ignition
AHRR	Apparent heat release rate
AI	Auto-ignition
aTDC	After top dead centre
CA	Crank angle
CA50	CA location at 50% heat release point
CAI	Controlled auto-ignition
CHR	Cumulative heat release
EoLTHR	End of LTHR
GDI	Gasoline direct injection
HR	Heat release
HTHR	High temperature heat release
ICE	Internal combustion engine
ID	Ignition delay
LT	Low temperature
LTHR	Low temperature heat release
LW	Livengood-Wu
NO_x	Oxides of nitrogen
NTC	Negative temperature coefficient
P	Pressure
PRF	Primary reference fuel
PSHR	Pre-spark heat release
Q_{hr}	Heat release
Q_{ht}	Heat transfer
rpm	Revolutions per minute
SI	Spark ignition
SoLTHR	Start of LTHR
T	Temperature
t	Time
T_{in}	Inlet air temperature
TDC	Top dead centre
V	Volume

References

1. K. Senecal and F. Leach, *Racing Toward Zero: The Untold Story of Driving Green*. SAE International, Jun 2021.
2. W. P. Attard and H. Blaxill, "A lean burn gasoline fueled pre-chamber jet ignition combustion system achieving high efficiency and low nox at part load," in *SAE 2012 World Congress and Exhibition*, SAE International, apr 2012.
3. W. R. Leppard, "The chemical origin of fuel octane sensitivity," in *International Fuels and Lubricants Meeting and Exposition*, SAE International, oct 1990.
4. P. Saisirirat, F. Foucher, S. Chanchaona, and C. Mounaïm-Rousselle, "Effects of ethanol, n-butanol — n-heptane blended on low temperature heat release and hrr phasing in diesel-hcci," in *9th International Conference on Engines and Vehicles*, Consiglio Nazionale delle Ricerche, sep 2009.
5. M. U. Waqas, A. Hoth, C. P. Kolodziej, T. Rockstroh, J. P. Gonzalez, and B. Johansson, "Detection of low temperature heat release (lthr) in the standard cooperative fuel research (cfr) engine in both si and hcci combustion modes," *Fuel*, vol. 256, p. 115745, 2019.
6. G. Shibata, K. Oyama, T. Urushihara, and T. Nakano, "Correlation of low temperature heat release with fuel composition and hcci engine combustion,," *SAE Technical Paper*, 2005.
7. D. A. Splitter, A. Gilliam, J. Szybist, and J. Ghandhi, "Effects of pre-spark heat release on engine knock limit," *Proceedings of the Combustion Institute*, vol. 37, no. 4, pp. 4893–4900, 2019.
8. D. A. DelVescovo, D. A. Splitter, J. P. Szybist, and G. S. Jatana, "Modeling pre-spark heat release and low temperature chemistry of iso-octane in a boosted spark-ignition engine," *Combustion and Flame*, vol. 212, pp. 39–52, 2020.
9. D. Splitter, B. Kaul, J. Szybist, and G. Jatana, "Engine operating conditions and fuel properties on pre-spark heat release and spi promotion in si engines," *SAE International Journal of Engines*, vol. 10, no. 3, pp. 1036–1050, 2017.
10. Z. Hu, J. Zhang, M. Sjöberg, and W. Zeng, "The use of partial fuel stratification to enable stable ultra-lean deflagration-based spark-ignition engine operation with controlled end-gas autoignition of gasoline and e85," *International Journal of Engine Research*, vol. 21, no. 9, pp. 1678–1695, 2020.
11. M. Yamakawa, T. Youso, T. Fujikawa, T. Nishimoto, Yoshitaka, gt;Wada, K. Sato, and H. Yokohata, "Combustion technology development for a high compression ratio si engine," *SAE International Journal of Fuels and Lubricants*, vol. 5, no. 1, pp. 98–105, 2012.
12. C. R. Stone, *Introduction to Internal Combustion Engines*. Macmillan International Higher Education, 4 ed., 2012.
13. F. Leach, R. Stone, M. Davy, and D. Richardson, "Comparing the effect of different oxygenate components on pn emissions from gdi engines," 12 2015.
14. F. C. Leach, M. Davy, and B. Terry, "Combustion and emissions from cerium oxide nanoparticle dosed diesel fuel in a high speed diesel research engine under low temperature combustion (ltc) conditions," *Fuel*, vol. 288, p. 119636, 2021.
15. N. Papaioannou, F. C. Leach, M. H. Davy, A. Weall, and B. Cooper, "Evaluation of exhaust gas recirculation techniques on a high-speed direct injection diesel engine using first law analysis," *Proceedings of the Institution of Mechanical*

Engineers, Part D: Journal of Automobile Engineering, vol. 233, no. 3, pp. 710–726, 2019.

16. F. Leach, R. Ismail, M. Davy, A. Weall, and B. Cooper, "Comparing the effect of fuel/air interactions in a modern high-speed light-duty diesel engine," in *13th International Conference on Engines and Vehicles*, SAE International, sep 2017.

17. D. Bresenham, J. Reisel, and K. Neusen, "Spindt air-fuel ratio method generalization for oxygenated fuels," *SAE Transactions*, vol. 107, pp. 2154–2171, 1998.

18. Y. Wu, P. Pal, S. Som, and T. Lu, "A skeletal chemical kinetic mechanism for gasoline and gasoline/ethanol blend surrogates for engine cfd applications," 5 2017.

19. T. Urushihara, T. Nakano, G. Shibata, and K. Oyama, "Correlation of low temperature heat release with fuel composition and hcci engine combustion," in *SAE 2005 World Congress and Exhibition*, SAE International, apr 2005.

20. J. Pan, P. Zhao, C. K. Law, and H. Wei, "A predictive livengood–wu correlation for two-stage ignition," *International Journal of Engine Research*, vol. 17, no. 8, pp. 825–835, 2016.

21. J. P. Szybist and D. A. Splitter, "Pressure and temperature effects on fuels with varying octane sensitivity at high load in si engines," *Combustion and Flame*, vol. 177, pp. 49–66, 2017.

Contact Information

Felix Leach
Department of Engineering Science,
University of Oxford,
Parks Rd,
Oxford,
OX1 3PJ,
UK
felix.leach@eng.ox.ac.uk

Acknowledgements

This research was funded in whole or in part by the Engineering and Physical Sciences Research Council Prosperity Partnership, grant number EP/T005327/1. For the purpose of Open Access, the author has applied a CC BY public copyright licence to any Author Accepted Manuscript (AAM) version arising from this submission. The Prosperity Partnership is a collaboration between Jaguar Land Rover, Siemens Digital Industries Software, the University of Bath, and the University of Oxford. The authors would also like to thank the Dept. of Engineering Science technicians and maintenance teams for facilities support. Due to confidentiality agreements with research collaborators, data supporting this paper can only be made available to bona fide researchers subject to a non-disclosure agreement. Details of the data and how to request access are available from the "Oxford Research Archive" repository at https://ora.ox.ac.uk/.